SEMARAK ILMU PUBLISHING

CFD Letters

Journal homepage:
https://semarakilmu.com.my/journals/index.php/CFD_Letters/index
ISSN: 2180-1363

Impact Tip Speed Ratio in Performance Analysis for Horizontal Axis Wind Turbine (HAWT) with Optimal Twist and Tapered (OPT) Blade Shape

Muhammad Al,Ain Mat Zin[1], Izuan Amin Ishak[1,*], Mohammad Arafat[1], Nor Afzanizam Samiran[2], Norain Sahari[3]

[1] Department of Mechanical Engineering Technology, Faculty of Engineering Technology, Universiti Tun Hussein Onn Malaysia, 84600 Pagoh, Johor, Malaysia
[2] Department of Mechanical Technology, Faculty of Mechanical and Manufacturing Engineering, Universiti Tun Hussein Onn Malaysia, 86400 Parit Raja, Batu Pahat, Johor, Malaysia
[3] Department of Electrical Engineering Technology, Faculty of Engineering Technology, Universiti Tun Hussein Onn Malaysia, 84600 Pagoh, Johor, Malaysia

ARTICLE INFO

Article history:
Received 6 September 2023
Received in revised form 9 October 2023
Accepted 12 November 2023
Available online 31 March 2024

Keywords:
OPT; HAWT; TSR

ABSTRACT

Performance for Horizontal Axial Wind Turbine (HAWT) is influenced by the difference in tip speed ratio (TSR) and mesh distribution. The objective of this article is to study the optimal performance of wind turbines when subjected to different mesh resolution, TSR and wind speed velocity.Therefore, it is important to study the effects of different mesh resolutions in terms of wind turbine performance. To achieve that, a 0.65m optimal twist and tapered (OPT) blade is used with various inlet velocities and TSR. This study uses the k-ω shear-stress transport (SST) based Reynold-Average Navier Stokes (RANS) approach in commercial ANSYS Fluent CFD software. This simulation was performed using the Moving Ratio Frame (MRF) method. To find the optimum grid resolution, a Grid Independence Test (GIT) was conducted comparing the coefficient of power (C_p). From the RESULT, TSR 6 shows the best HAWT performance when C_p for inlet velocity 8 m/s is 0.2608.

1. Introduction

This study focuses on the performance of small HAWT blades when different TSRs are applied with appropriate meshing sizes. HAWT blade allows wind resources to be abstracted into electricity for use in community life and industry to avoid pollution because the resulting electricity source is primarily from fossils. The electricity produced depends on the performance of a wind turbine. Among the factors that affect HAWT performance are the use of the TSR ratio and blade radius size. The size of the blade determines the surface area that will be swept to extract the electricity generated with the speed of the blade determined by the TSRs. Based on previous studies, HAWT performance is affected by TSR, where the energy produced increases. Still, when it reaches the optimal level of the wind turbine, the power starts to decrease [1]. Based on the type of airfoil profile

* *Corresponding author.*
E-mail address: izuan@uthm.edu.my (Izuan Amin Ishak)

https://doi.org/10.37934/cfdl.16.8.1832

design code employed, the blade element momentum (BEM) method is utilized to produce the kind of blade suitable for use [2]. Currently, the utilization of BEM is still adaptable for advancing numerical studies for aerodynamic HAWT features, performed at different levels and ranges followed by CFD computation.

The specification of the blades is one of the elements that affect wind turbine performance. Many different designs of wind turbines are employed nowadays, but the Horizontal Axial Wind Turbine (HAWT) and the Vertical Axial Wind Turbine are among the ones that are frequently contested (VAWT). The difference between HAWT and VAWT is that the wind for HAWT travels parallel to the blade, whereas the wind for VAWT can flow from different angles. When its efficiency reaches 50%, HAWT is suitable for considerable capacity needs as opposed to VAWT, which can only obtain 40% [3]. When compared to VAWT, which has a capacity of only 6 Mw, modern HAWT has a 20 Mw capacity, meaning that the power coefficient (C_p) is 2 % higher in HAWT [3]. Additionally, HAWT is separated into many blade types, including optimal and tapered (OPT), untampered and optimal twist (UOT), and untampered and untwisted (UUT) [4, 5]. The next difference between the two kinds of blades is that OPT has various chord length sizes in each section compared to UOT and UUT, whereas OPT and UUT have different twist angles [4, 5].

OPT displays a greater C_p in terms of blade performance than UUT and UOT [4]. This is also a result of the chord length and twist angle factors. Earlier research examined the performance of wind turbines based on twist angle and various chord length sizes at the designated radial position [6]. The C_p drops to -1.2 when the wind speed hits 10 m/s when the twist angle is reduced to -25% and increased to 25% [6]. However, it was discovered that the C_p achieved the ideal level of 0.5 at a wind speed of 3 m/s [6]. The speed at which the blade rotor rotates in the swept area affects blade performance. Tip speed ratio (TSR) is a technique used to assess a wind turbine's power output. Previous research has connected TSR and C_p with the variation in blade diameter [7, 8]. According to the study, four and five blades at TSR 5 reached their best performance when they were close to C_p 0.5, but their performance fell as TSR increased [7]. Compared to three blades operating at their optimum C_p of 0.5 from TSR 7 to TSR 15 [7]. Below three blades below show a lower optimal level [7]. This shows that when the blade rotation rotor is raised based on TSR, blade three can provide a larger C_p than other blades.

When a twist angle is employed to create the turbine blades, the angle of attack is the angle formed by the chord line and the incoming wind. With the least amount of drag, the most precise angle of attack helps provide the highest lift [9-11]. When the lift coefficient is good and the drag coefficient is low, the NACA 4418 airfoil exhibits suitability for applications in the construction of turbine blades [9]. CFD simulation techniques have also been utilized in earlier research to examine the performance of wind turbines, the choice of airfoil profiles, the impact of the number of blades being employed, and pitch angle variations [12-17]. Previous research has used the GIT technique to choose a quality mesh while also reducing time to ensure that the data obtained reaches the actual reading [18, 19]. The performance data of OPT blades, flow structure blades, and parameters influencing the performance of blades based on wind speed generated by CFD simulation in this study.

The objective of this study will be to see the optimal performance of wind turbines when subjected to different wind speeds, TSR, and mesh sizes. Based on this difference, the study can find out energy capture and efficiency when changes in TSR affect wind turbine energy. The study also focuses on the HAWT's effect output, torque, and overall efficiency with optimized blades. TSR is also influenced by aerodynamic performance to analyze how the blades' design and optimization affect the turbine's ability.

2. Methodology

2.1 Wind Turbine Specification

Wind turbines feature components that ensure their movement, including airfoils, the best possible blade design, and wind turbine blades that are attached to rods, shafts, and hubs [20]. Calculating wind turbine power (*P*) at rated wind speed (*v*) will yield the rotor blade diameter [5]. The 300-watt HAWT from the previous research will be simulated using the ANSYS FLUENT program with different wind speeds and TSR. The calculation determined that the length of the blade is 650 mm by taking into consideration different system component efficiencies and entering the value of 8 m/s into [2]. OPT blade design uses BEM theory with chord values and twist angles for chords as in Table 1. Table 1 shows information for 1 OPT blade with each section as in Figure 1 having its airfoil distance with different chord sizes and twist degrees. Due to its high lift and low drag coefficients, small HAWT blades frequently utilize the NACA 44xx and NACA 230xx family airfoils [21]. The NACA 4418 was employed in this study, with a maximum lift-to-drag ratio of 44.447, which equates to an angle of attack of 6.5° and a lift coefficient of 1.209.

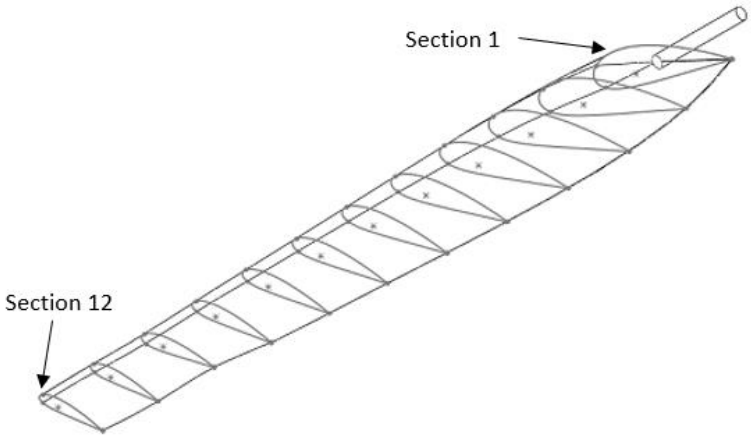

Fig. 1. Optimal twist and tapered (OPT) blade for small HAWT

The National Advisory Council for Aeronautics (NACA) develops airfoil profiles by assigning a numerical code to the cross-section after assessing its attributes and the letters NACA [22]. Different regulations are used for symmetric and chambered airfoils; for symmetry, the code is NACA 00xx, where xx is the chord thickness ratio [22]. NACA 0012, for example, represents a chord whose thickness is 12% of its length [22]. The most straightforward asymmetric system is used by chambered airfoils, which use the asymmetric 4-digit NACA. The first figure provides information about the chamber percentage, and the second digit includes information about the maximum camber along the foil chord. In contrast to chord length, numbers three and four have chord thickness [22]. The NACA 4418 airfoil shows that it has a chamber percentage of 4% and can reach a maximum chamber of 40%. The maximum chamber is 40% with 0018 symmetry of thickness 185 of the chord length, and the chamber percentage has a specific meaning on the first digit [22]. Figure 2 depicts the formation of the airfoil profile. According to the NACA code, the first four characters of the chord for NACA 4418 represent 40% of its chord (0.4) from X coordinates (1,0). The chord's length is used as a reference when forming the OPT blade, the chord's length is used as a reference.

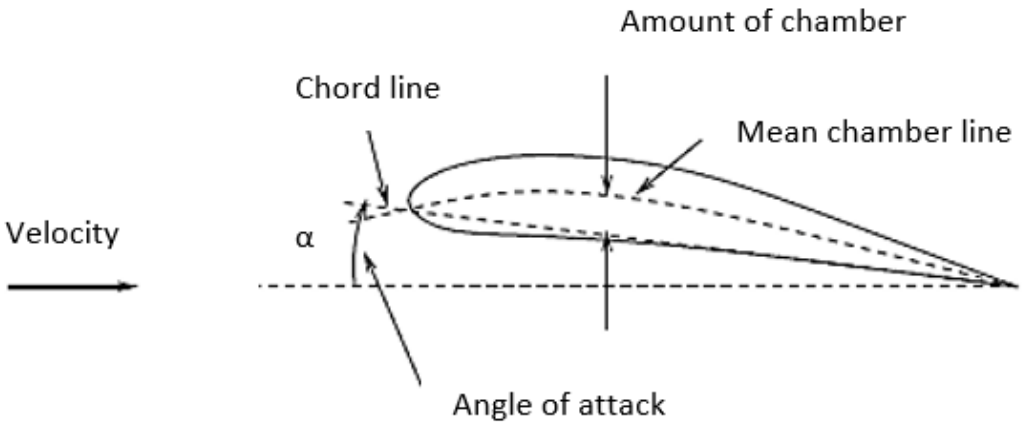

Fig. 2. Nomenclature of an airfoil

The blade element momentum (BEM) theory is used to design the optimum blade shape. The blade chord length and twist distributions along the span are calculated at design TSR and design angle of attack. Tip speed ratio (λ) is an important parameter in the design procedure, and it is the ratio between tip speed and wind speed. As given by Eq. (1), The optimal TSR depends on the number of blades (n). The blade is divided into twelve elements and twisted while the angle of attack remains constant at all elements; the velocities and the forces on the blade are shown in Figure 3. The relative wind angle (ϕ), the chord length (c) and the pitch angle (Θ_P) of the blade at every with element has been found. from Eq. (3), Eq. (4), and Eq. (5)[5].The chord and twist distribution for the OPT blade are abbreviated in Table 1.

$$\lambda = \frac{\omega.R}{v} \tag{1}$$

$$\varphi_i = \left(\frac{2}{3}\right).tan^{-1}\left(\frac{1}{\lambda_{r,i}}\right) \tag{2}$$

$$\theta_{p,i} = \varphi_i - \alpha_{design,i} \tag{3}$$

$$c_i = \frac{8.\pi.r_i}{n.C_{l,design,i}} \times (1 - cos\varphi_i) \tag{4}$$

$$\lambda_r = \lambda.\left(\frac{r}{R}\right) \tag{5}$$

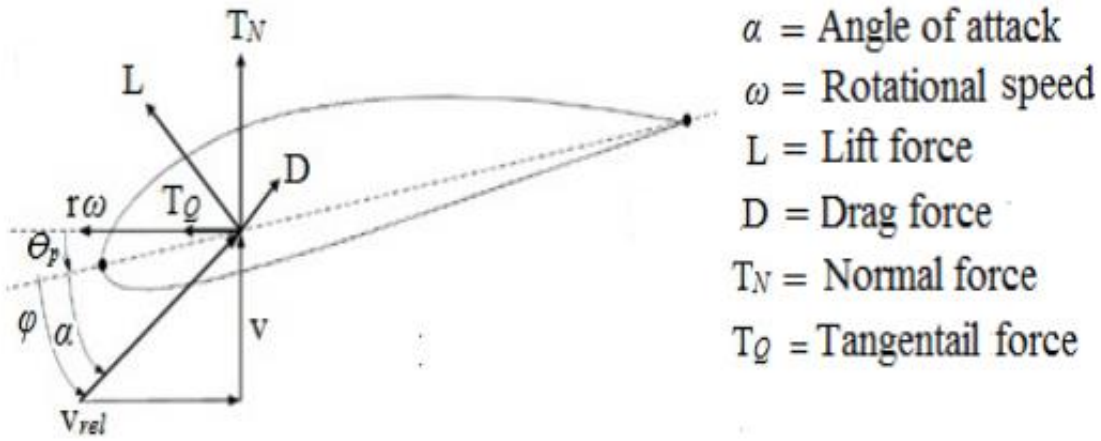

Fig. 3. Schematic of angles and forces on blade element [5]

Table 1
Chord and Twist distribution for OPT blade

Section number	Radius *r* (m)	Chord *c* (m)	Twist angel Θ_p (deg)
1	0.10	0.153800	32.42800
2	0.15	0.153400	25.02700
3	0.20	0.140900	19.56200
4	0.25	0.126300	15.50000
5	0.30	0.112800	12.46000
6	0.35	0.101100	10.10300
7	0.40	0.091200	8.23900
8	0.45	0.082845	6.73680
9	0.50	0.075500	5.50277
10	0.55	0.069680	4.47330
11	0.60	0.064400	3.60000
12	0.65	0.059900	2.85700

2.2 CFD Modelling and Analysis

The complete shape of the horizontal wind turbine with OPT blades based on NACA 4418 is depicted in Figure 4. Based on the HAWT hub, there are 120 degrees between the OPT blades with a diameter of 1.3 meters. Airfoil coordinates are essential to form an edge in Solid-Work software before completing a HAWT with improvements in ANSYS Space Claim R. Then, CFD modeling will be done using this schematic. Figure 4 also displays the assembly for the isolated rotor and complete turbine types. The control volume comprises two cylinders with a 4 m diameter (d_{cv}) and 10 m length (l_{cv}) that operate as a virtual wind tunnel when stationary. The other is a rotating cylinder made around HAWT with dimensions of 1.34 meters in diameter (d_{cv}) and 0.13 meters in length (l_{cv}).

Due to the focus on the fluid surrounding the HAWT in the present study, the HAWT model approaches the fine mesh using a specific size. In regions other than HAWT, the coarse mesh is utilized, as depicted in Figure 5. Tetrahedral elements were used to mesh the internal and external usage volumes, which have approximately 1,786,902 cells for the rotating zone and 1,900,815 cells for the entire turbine module.

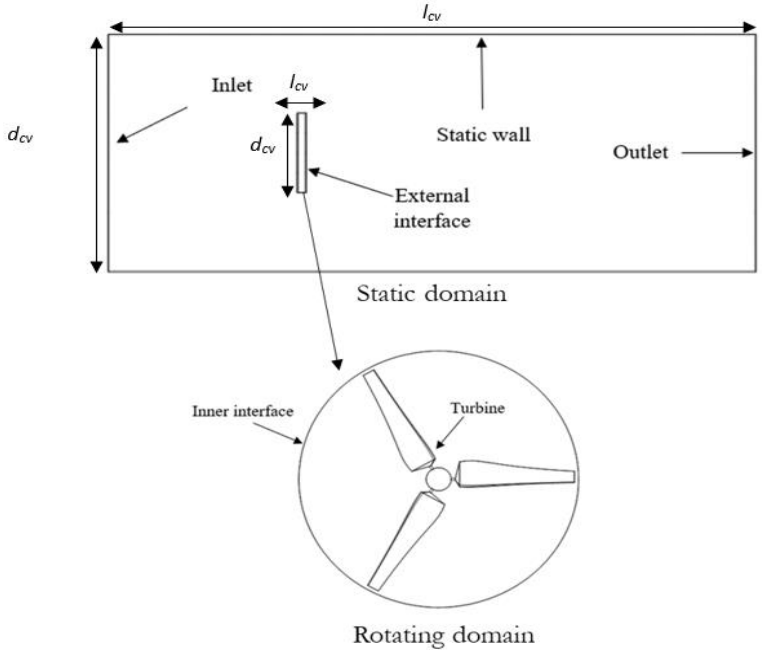

Fig. 4. Computational domain indicating the boundary conditions

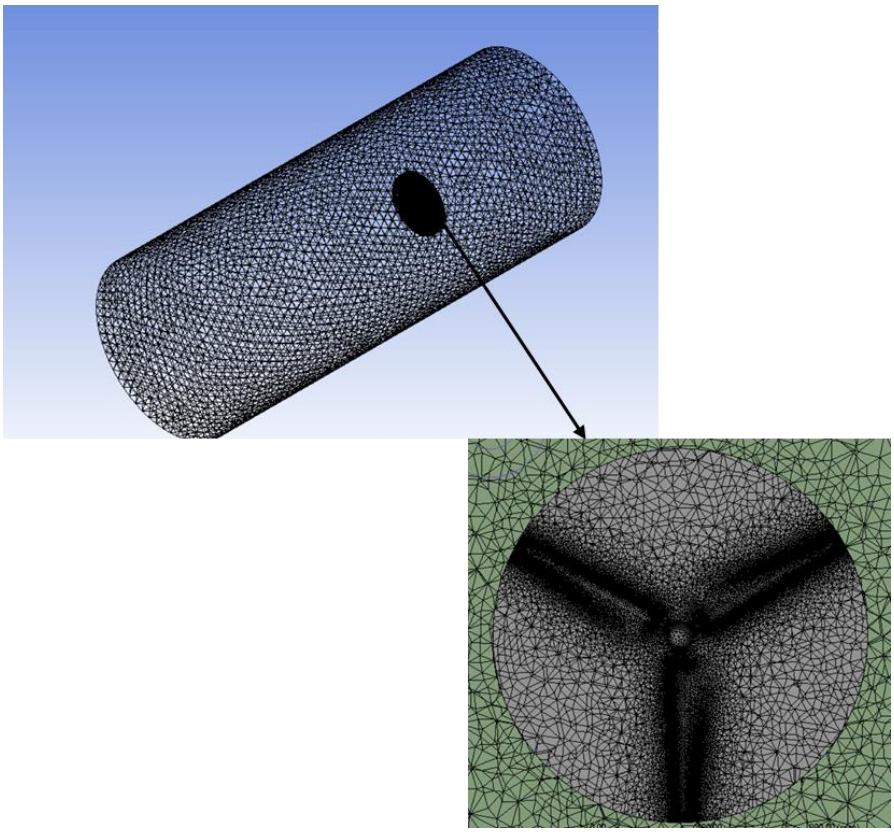

Fig. 5. Mesh isometric view and tetrahedral mesh around the blade

The wind turbine is simulated using the setup solver according to the required scenario. The moving reference frame (MRF) approach is employed in this solver setup because it can be used for rotating models. The study will use the torque data obtained from this simulation to calculate the energy produced by the wind turbine and its performance. To understand the time average flow physics around the wind turbine, the steady mode of the simulation utilizing a Shear Stress Transport or SST-based Delayed Reynold averaged Navier Stokes (RANS) turbulence model is used. The SIMPLE approach is applied for pressure velocity coupling. The entire set of simulation examples was run utilizing a parallel computing approach. During the solution process, six logical processors were used. The RANS formulation can be written as Eq. (6) and Eq. (7). A summary of the solver simulation setting can be seen in Table 2.

$$\nabla . \vec{V} = 0 \tag{6}$$

$$\rho \frac{D\vec{V}}{Dt} = -\nabla p + \rho \vec{g} + \mu \nabla^2 \vec{V} \tag{7}$$

Momentum Eq. (7) is a vector equation obtained by applying Newton's Law of motion to a fluid element. It is supplemented by the continuity Eq. (6) and the energy equation. The momentum equation is the total derivative of change velocity with time. Pressure gradient (∇p) is fluid flows in the direction of the most significant change in pressure. Body force term ($\rho \vec{g}$) is external forces that act on the fluid, and diffusion term ($\mu \nabla^2 \vec{V}$) is a newton fluid, viscosity operates as a diffusion of momentum.

Table 2
Specifications solver setup

Solver settings	Description
Mode	Moving reference frame (MRF)
Iteration	1200
Turbulence model	*k-ω* shear stress transport (SST)
Method	SIMPLE coupling
Inlet velocity (m/s)	5, 6, 8, 10,12, 14, 15
Outlet	Air pressure
Density of air kg/m3	1.225 kg/m3
Viscosity ratio	10%
Intensity Ratio	10%
Solver settings	Description

2.3 Grid Independence Test

Based on the evaluation of various grid conditions, the grid independence test is used to identify the best grid condition with the fewest grids without producing a difference in the numerical results [14]. Table 3 lists the parts of the wind turbine that change in size, with M2 being half as large as M1 and so on through M4. The total number of elements also varies depending on the change in element size, as indicated in Table 3. The grid independence test (GIT) utilizes the size difference of each HAWT component to detect non-significant difference values, ensuring that the data obtained meets the best level of accuracy.

Figure 6 displays the results of TSR against the coefficient of power C_p for different mesh resolutions. It can be shown that when the M1 difference between two meshing does not reach the same value as the other meshing, it exhibits a large difference value. Graph curvature for M2, M3, and M4 is nearly identical, except for TSR 2 and TSR 3. TSR 6 has been selected to compare the error percentages of the four meshes to determine the ideal power value generated by OPT for this investigation. At TSR 6, M1 = 0.2493, M2=0.2608, M3 = 0.2605, and M4 = 0.2590 were the C_p values.

In Figure 7, it can be seen that the percentage difference between M1 and M2 was 4.6%, M2 and M3 were 0.11%, and M3 and M4 were 0.73%. M2 was selected as the element size for this investigation based on the data collected since M2 and M4 likewise had a percentage difference of 0.69%. The contrast of 0.69% below 1% shows a slight error difference for M2 and M4. 0.69 % with this small difference, the choice of M2 was used for time savings and, it was also chosen because of its standard computer specifications. Due to the restrictions of the computer simulation that was employed, this enables studies to be developed and used faster. Figure 8 shows important components with numbers that can be referenced in Table 3 using the selected mesh size elements M2.

Table 3
Types of element sizes for four different meshes

	Component	M1	M2	M3	M4
Element size (mm)	1. Blade surface	120.0	60.00	30.000	15.0000
	2. Cylindrical root section	30.0	15.00	7.500	3.7500
	3. Hub	60.0	30.00	15.000	7.5000
	4. Airfoil shape	4.2	2.10	1.050	0.5250
	5. Trailing edge	1.5	0.75	0.375	0.1875
	6. Round leading edge	4.2	2.10	1.050	0.5250
	Number of elements	890,428	1,900,131	4,508,137	11,433,609

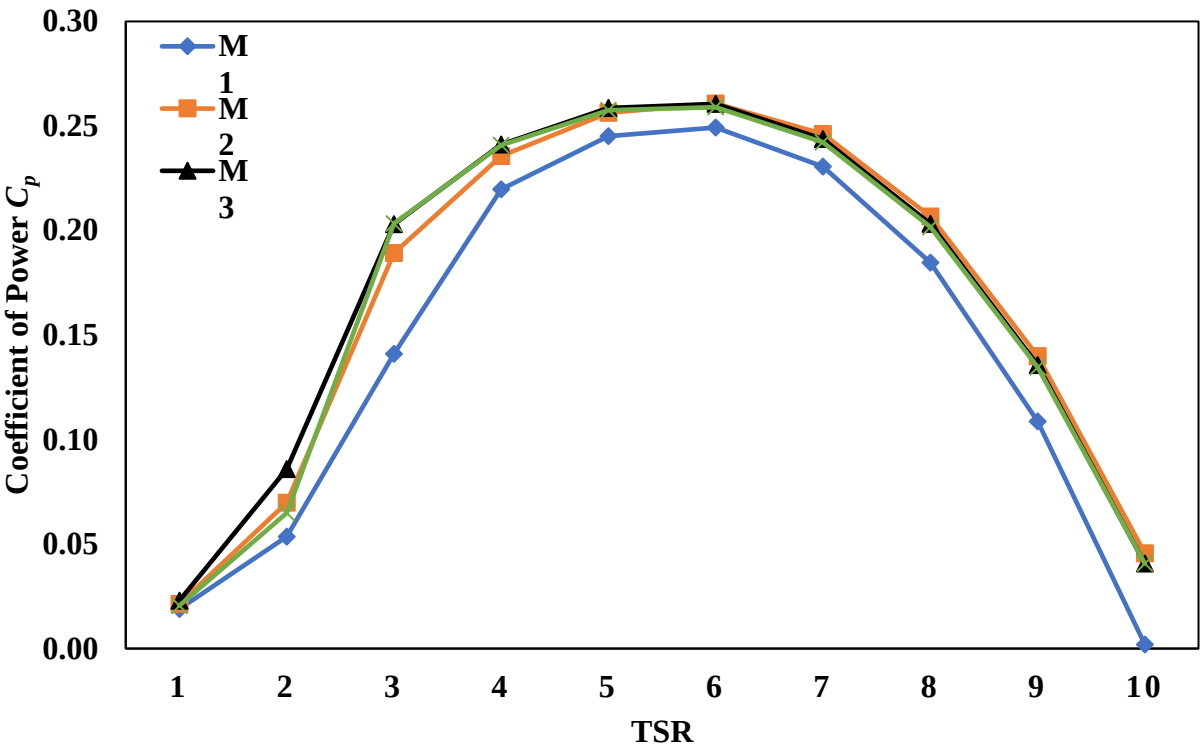

Fig. 6. Performance of coefficient of power (C_p) with TSR for different mesh resolutions

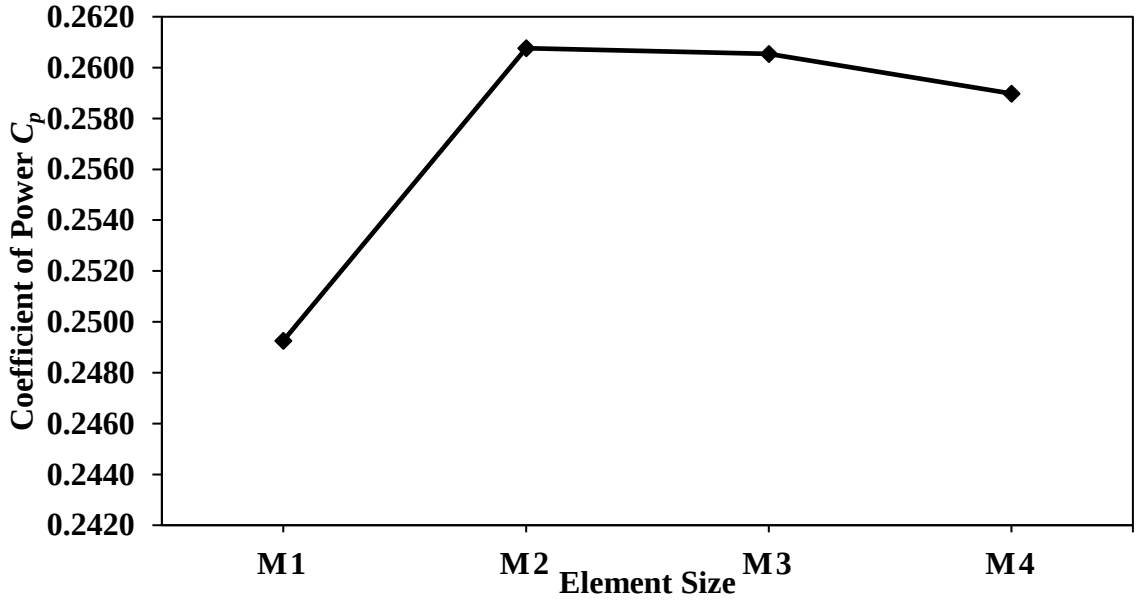

Fig. 7. Grid independence test based on the coefficient of power (C_p) at TSR = 6

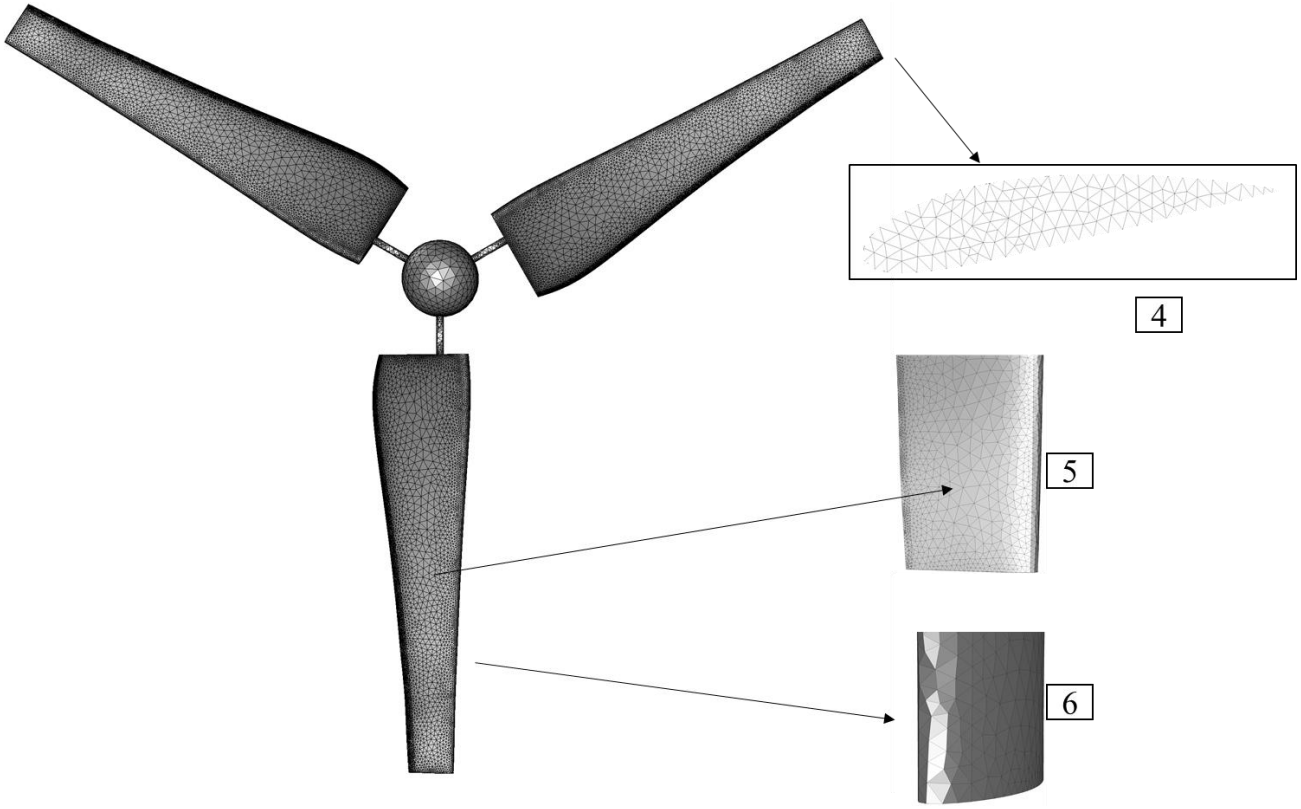

Fig. 8. Form OPT blade in M2

2.4 CFD Validation

The model OPT used in the experimental and CFD simulations is checked using validation processes to ensure they are relatively near the same values. The investigation will be able to measure the error value that will be obtained by comparing simulation and experimental results from previous research. The validation of the current study is compared with the published results [5, 23]. Figure 9 illustrates how the power output achieved through CFD simulations carried out in this study based on various wind speeds may be compared with the power output provided by previous publications [5, 23]. This demonstrates that the current model is appropriate for simulating the other CFD examples in the project. In general, it can be concluded that the present study blends well with the previous result. Based on the difference between Abdel Rahman [5], the most minor percentage difference is 0.61% at a wind speed of 8 m/s, while the most significant percentage difference is 14.23% at 10 m/s. Based on the wind turbine's capacity, the CFD simulation terminates when it reaches a power output of 300 watts. Hence, it is confirmed that the results are validated since the percentage errors are within acceptable ranges for different wind speeds. This demonstrates the efficacy of the existing model in simulating other CFD case models in current studies.

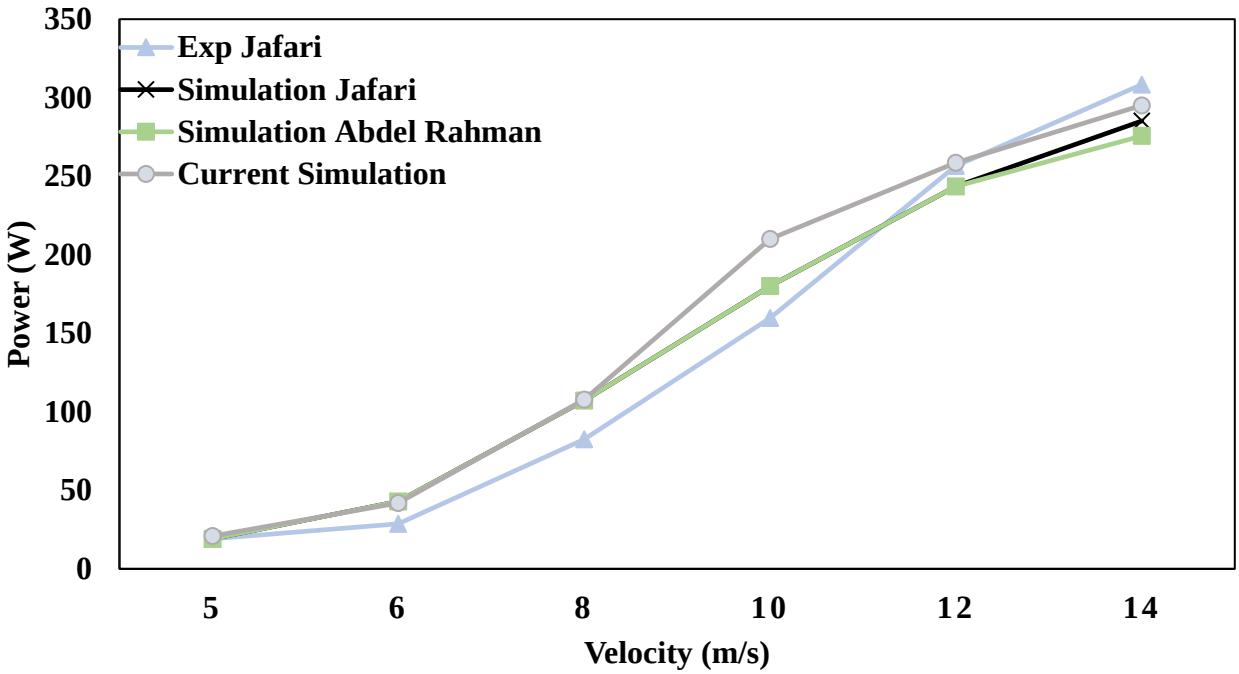

Fig. 9. Comparison between power output obtained by current CFD simulation, Jafari simulation and experimental [23], Abdel Rahman CFD simulation [5] versus the wind speeds

3. Results

3.1 Performance of OPT Blade with Different TSR

Figure 10 displays the data as a graph for TSR and various velocities from the wind turbine simulation. The graph pattern for speeds of 5 m/s and 8 m/s reveals an upward trend in the curve up to the optimal point at TSR 6, then a downward trend till TSR 10. The 8 m/s velocity curve pattern indicates a higher speed than 5 m/s. This pattern demonstrates how well wind turbines operate in producing energy. The relationship between wind speed and TSR is that TSR is the ratio of wind turbine blade rotation speed. The higher the TSR, the higher the rotation of the wind turbine blade. This graph illustrates that the wind turbine's performance is at its peak at TSR 6, where the C_p value is 0.0986 for 5 m/s and 0.2608 for 8 m/s. The wind turbine initially produces little energy, with C_p for 5 m/s = 0.0082 and 8 m/s = 0.0214 at TSR 1, before reducing once more at TSR 10 with 5 m/s = 0.0097 and 8 m/s = 0.0455. Additionally, this demonstrates that as wind speed increases, the value of C_p rises as well. This is demonstrated by the fact that at a wind speed of 8 m/s as opposed to 5 m/s, C_p rises by 164.5%. The increase in TSR and wind speed is hence the factor that influences the wind turbine's performance.

This graph illustrates that the wind turbine's performance peaks at TSR 6, where the C_p value is 0.0986 for 5 m/s and 0.2608 for 8 m/s. The wind turbine initially produces little energy, with C_p for 5 m/s = 0.0082 and 8 m/s = 0.0214 at TSR 1, before reducing once more at TSR 10 with 5 m/s = 0.0097 and 8 m/s = 0.0455. Additionally, this demonstrates that as wind speed increases, the value of C_p also rises. This is shown by the fact that at a wind speed of 8 m/s instead of 5 m/s, C_p rises by 164.5%. The increase in TSR and wind speed is, hence, the factor that influences the wind turbine's performance.

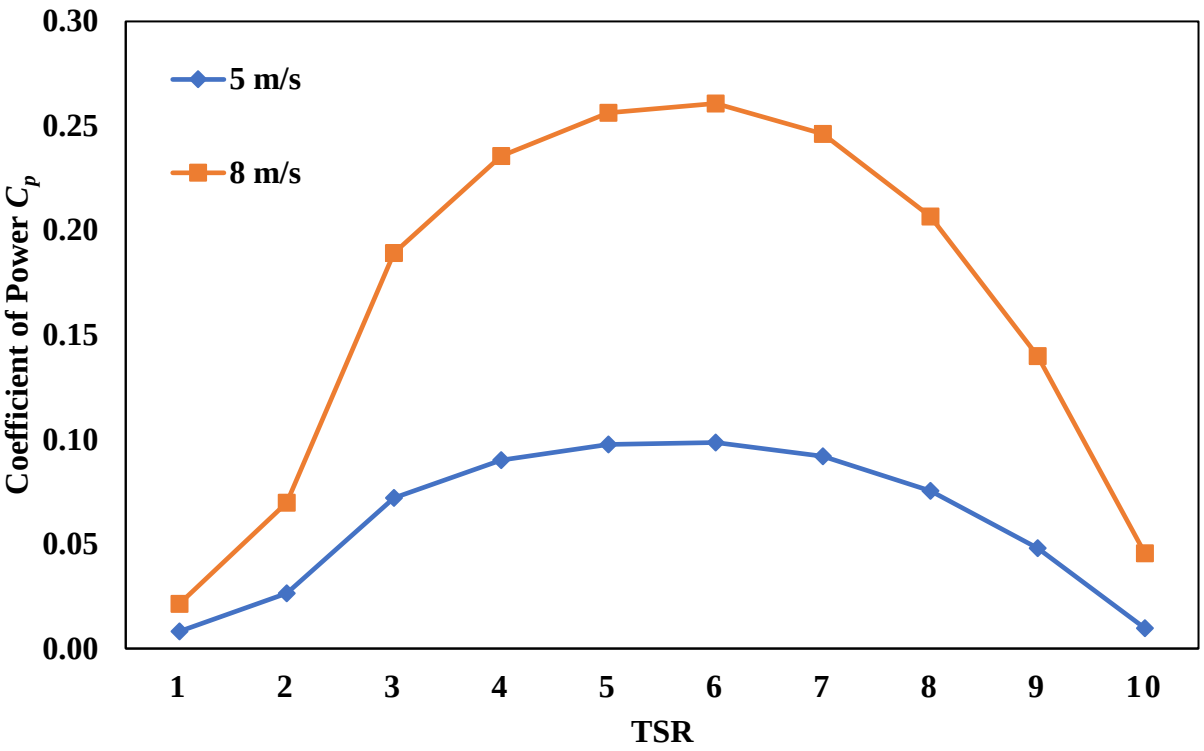

Fig. 10. Performance OPT with different TSR at V = 5 m/s and V = 8 m/s

3.2 Flow-structure OPT HAWT

In this subsection will be discussed about pressure distribution and velocity distribution.

3.2.1 Pressure distribution

Figure 11 illustrates the blade pressure distribution after analysis to reveal its function in predicting thrust and power. When the velocity is 8 m/s, the pressure coefficient contour is normalised by a low of -400 Pa and a maximum of 350 Pa. The findings indicate that the flow standstill caused a significant pressure on the leading edge of the entire blade. The twisting of the blades causes the lift contribution to the power production to decrease from root to tip, and the reverse pattern is anticipated for the thrust contribution. For instance, at a radius of 0.55 m, the cross-section of the edge is virtually parallel to the plane of rotation, meaning that lift mostly contributes to thrust. Moreover, taking the chord's length into account.

The drag on the blade is caused by the pressure differential between the leading and trailing edges. Figure 11 also depicts the pressure distribution for the three different types of TSR. Comparing TSR 10 to TSR 6 and TSR 3, it can be said that TSR 10 generates a higher push. TSR 10 displays a low-pressure distribution area at 0.55 m. The location is anticipated because the wind is blowing so quickly that the top airfoil is under less pressure than the bottom. The branch is lifted into the air by the force of the wing due to the pressure difference. Additionally, this application is used for 0.3 5m and 0.15 m. 0.35 m and 0.15 m do not create the same pressure distribution as 0.55 m when observed at TSR 10. This is brought on by the variation in airfoil size, angle, and distance from the hub. Figure 12 shows a comparison between a pressure distribution with a constant radius and two velocities, 5 m/s and 8 m/s. The comparison reveals that compared to 5 m/s, 8 m/s has a wider low-pressure region above the airfoil surface. The blade can rotate more quickly with an airfoil at 8 m/s than at 5

m/s. This enables the swept area to produce more energy while moving at that speed. In terms of blade radius, it demonstrates that the low-pressure region lies at 0.55 m.

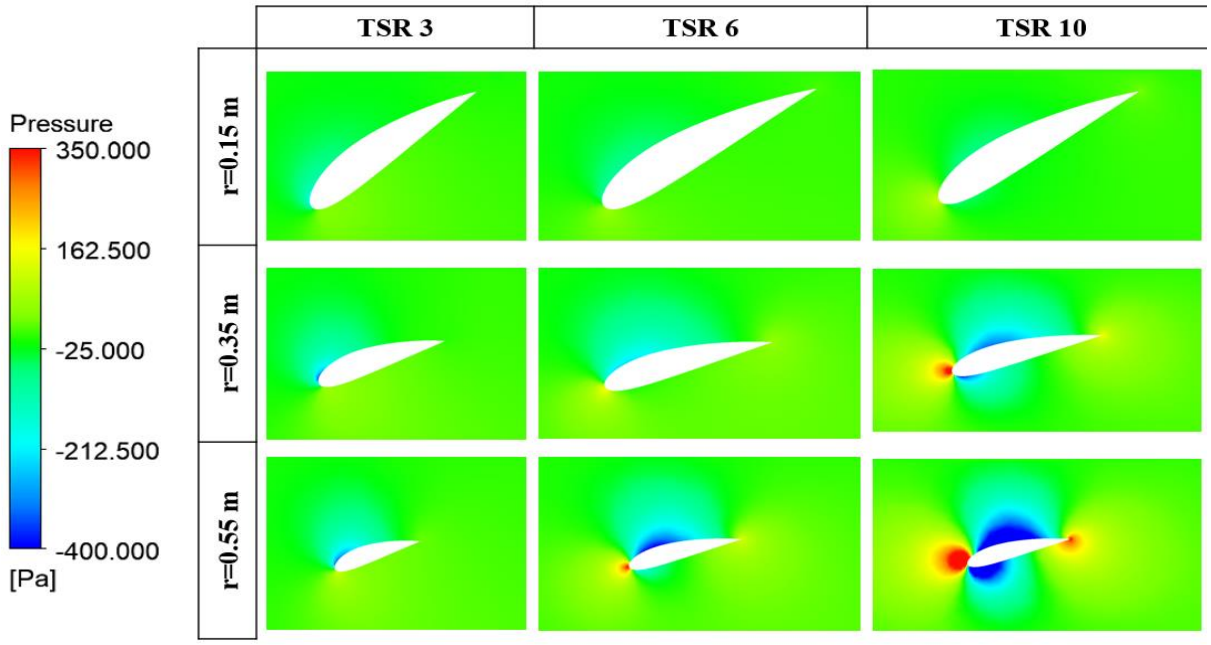

Fig. 11. Pressure distribution for different blade shapes in r = 0.15m, r = 0.35m and r = 0.55m at 8 m/s

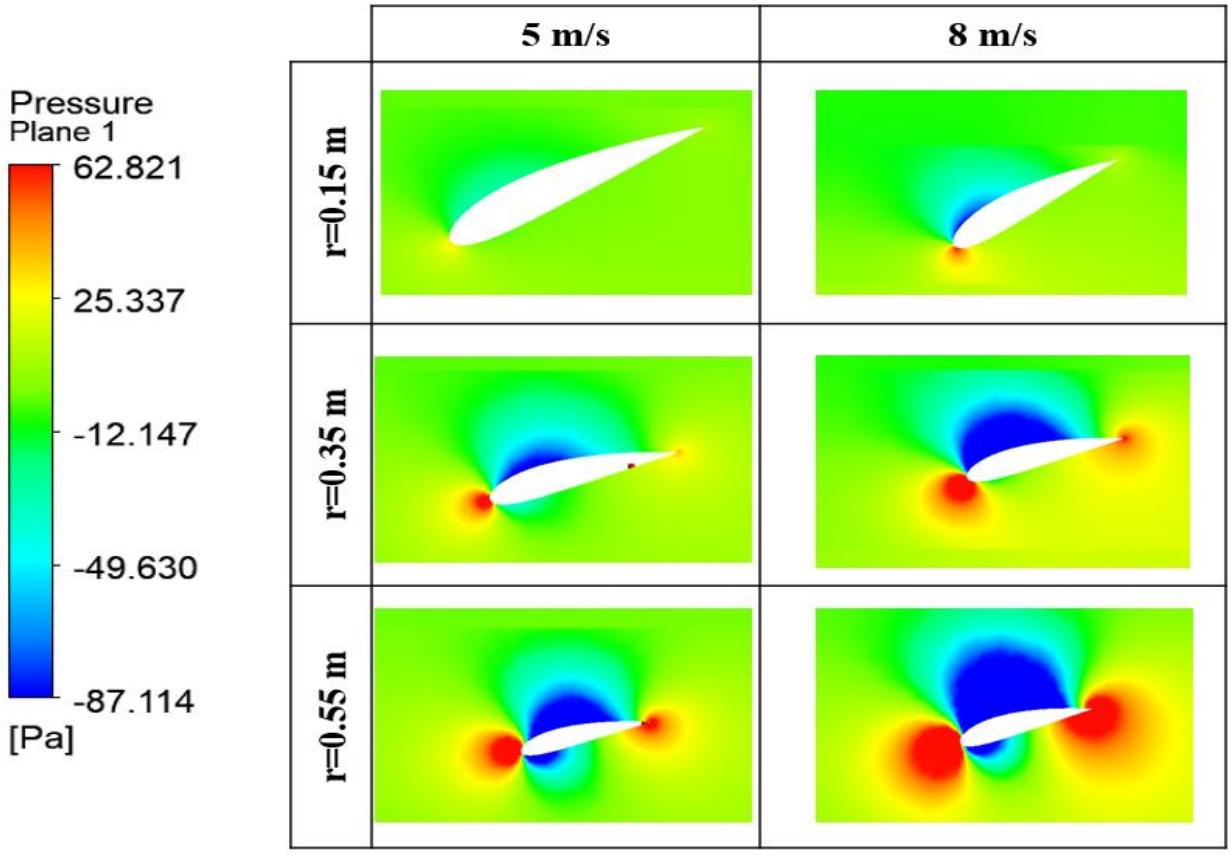

Fig. 12. Pressure distribution for different blade shapes in r = 0.15m, r = 0.35m and r = 0.55m at 5 m/s and 8 m/s

3.2.2 Velocity distribution

Figure 13 depicts the diagram of several OPT HAWT TSRs with a constant wind speed of 8 m/s. A minimum speed of 0 m/s and a top speed of 25 m/s are used to normalise the velocity coefficient contour. According to the comparison, TSR 10 has a high-velocity region spanning more than half of the blade. Compared to TSR 6 and TSR 3, the blade rotation of TSR 10 is higher. This demonstrates proof that the low-pressure region in Figure 11 is affected by fast speed. Air pressure is lower in areas with higher wind speeds and vice versa. As a result, the air pressure will decrease as the wind speed increases. Three separate TSRs demonstrate that the HAWT at the tip has a greater rate. This is as a result of the twist angle, which facilitates lifting. The point of the rotor blade will also increase as the velocity does. More electricity is produced when wind speeds rise up to a cap known as the rated speed. The turbine's maximum or rated power is produced at this point.

The air density, blade size, and regional wind speed all impact how quickly a wind turbine rotates. The velocity distribution for two speeds, 5 m/s, and 8 m/s, is shown in Figure 14. This illustration demonstrates that TSR 8 has a high-velocity region near the tip instead of TSR 6's 5 m/s. Compared to 5 m/s, TSR 8 delivers a blade rotation to set a higher site and produce more power. Substantial performance comparison of wind turbines is shown in Figure 10. However, higher TSR does not guarantee optimal wind turbine performance, because it was found that TSR 10 has a low power coefficient as shown in Figure 10. In Figure 13, although TSR 10 shows a high velocity, allowing the blade to rotate faster, it cannot capture the swept area because it reaches the wind turbine limit. So, when the turbine speed increases, the efficiency goes down.

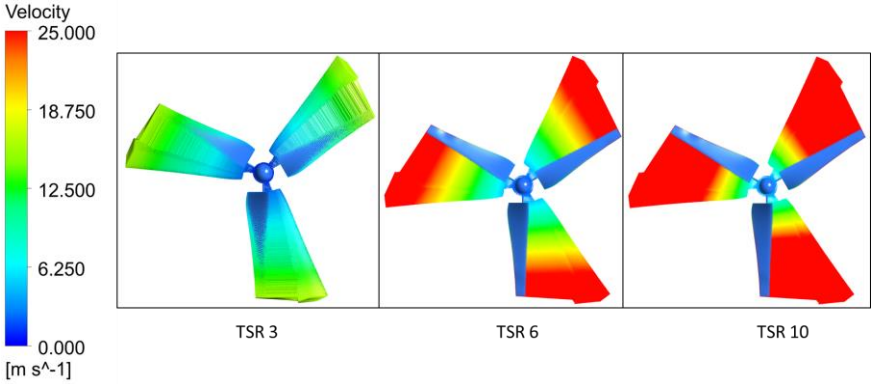

Fig. 13. Velocity distribution at wind speed 8 m/s at different TSR value

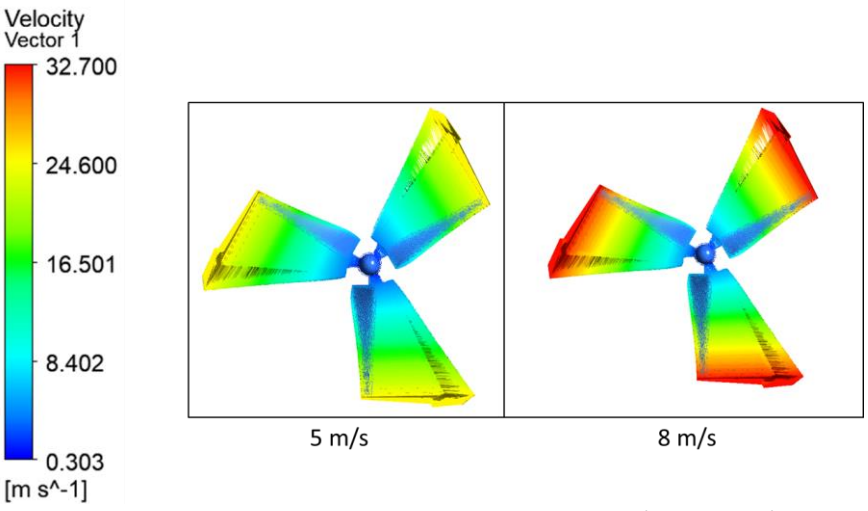

Fig. 14. Velocity distribution at wind speed 5 m/s and 8 m/s

4. Conclusions

In conclusion, this study achieved the main objective of finding the optimal performance design of HAWT OPT, which is seen when TSR 6 shows the optimal performance level. This study also found that when the wind velocity increases, the TSR value increases because the blade rotation speed increases with the increase in wind velocity. However, when the HAWT OPT reaches the limit, the wind velocity has no effect, and the performance value will decrease like TSR 10. The selection of twist angle and chord length is essential in the shape of the blade because it affects the performance. This is because the tip plays a role in ensuring the blade experiences lift. The fit of the airfoil shape on the lift should ensure that the upper part has a low-pressure distribution but a high-velocity distribution. A more in-depth study should be done to see the performance effect when the twist angle is changed to several values.

Acknowledgement

This research is financially supported by Universiti Tun Hussein Onn Malaysia under UTHM GPPS Grant (Q221). The author would also like to thank the Faculty of Engineering Technology, Universiti Tun Hussein Onn Malaysia for providing feasible research facilities for this study. Communication of the research is made possible through monetary assistance by Universiti Tun Hussein Onn Malaysia and the UTHM Publisher's Office via Publication Fund E15216.

References

[1] Suresh, A., and S. Rajakumar. "Design of small horizontal axis wind turbine for low wind speed rural applications." *Materials Today: Proceedings* 23 (2020): 16-22. https://doi.org/10.1016/j.matpr.2019.06.008

[2] Wang, Huimin, Jianliang Wang, Ji Yao, Weibin Yuan, and Liang Cao. "Analysis on the aerodynamic performance of vertical axis wind turbine subjected to the change of wind velocity." *Procedia Engineering* 31 (2012): 213-219. https://doi.org/10.1016/j.proeng.2012.01.1014

[3] Al-Rawajfeh, Mohammad A., and Mohamed R. Gomaa. "Comparison between horizontal and vertical axis wind turbine." *International Journal of Applied* 12, no. 1 (2023): 13-23. https://doi.org/10.11591/ijape.v12.i1.pp13-23

[4] Hsiao, Fei-Bin, Chi-Jeng Bai, and Wen-Tong Chong. "The performance test of three different horizontal axis wind turbine (HAWT) blade shapes using experimental and numerical methods." *Energies* 6, no. 6 (2013): 2784-2803. https://doi.org/10.3390/en6062784

[5] Abdelrahman, M. A., O. E. Abdellatif, M. Moawed, A. Eliwa, and Stanislav Mišák. "The CFD performance analysis for horizontal axis wind turbine with different blade shapes and tower effect." In *2015 16th international scientific conference on electric power engineering (EPE)*, pp. 754-759. IEEE, 2015. https://doi.org/10.1109/EPE.2015.7161197

[6] Purusothaman, M., T. N. Valarmathi, and S. Praneeth Reddy. "Selection of twist and chord distribution of horizontal axis wind turbine in low wind conditions." In *IOP Conference Series: Materials Science and Engineering*, vol. 149, no. 1, p. 012203. IOP Publishing, 2016. https://doi.org/10.1088/1757-899X/149/1/012203

[7] Adeyeye, Kehinde Adeseye, Nelson Ijumba, and Jonathan Colton. "The Effect of the Number of Blades on the Efficiency of a Wind Turbine." In *IOP Conference Series: Earth and Environmental Science*, vol. 801, no. 1, p. 012020. IOP Publishing, 2021. https://doi.org/10.1088/1755-1315/801/1/012020

[8] Fanel Dorel, Scheaua, Goanta Adrian Mihai, and Dragan Nicusor. "Review of specific performance parameters of vertical wind turbine rotors based on the SAVONIUS type." *Energies* 14, no. 7 (2021): 1962. https://doi.org/10.3390/en14071962

[9] Bayram, Halil. "Numerical investigation of airfoils aerodynamic performances." *International Journal of Energy Applications and Technologies* 9, no. 1 (2022): 1-5. https://doi.org/10.31593/ijeat.1033107

[10] Rubel, Robiul Islam, Md Kamal Uddin, Md Zahidul Islam, and M. D. Rokunuzzaman. "Numerical and experimental investigation of aerodynamics characteristics of NACA 0015 aerofoil." *International Journal of Engineering Technologies IJET* 2, no. 4 (2016): 132-141. https://doi.org/10.19072/ijet.280499

[11] Yang, Yunchao, and Gecheng Zha. "Super-lift coefficient of active flow control airfoil: What is the limit?." In *55th AIAA Aerospace Sciences Meeting*, p. 1693. 2017. https://doi.org/10.2514/6.2017-1693

[12] Shivsharan, Bhimrao A., Pramod B. Magade, Shrirang Chavan, and Sushilkumar Magade. "Experimental design, development and testing of novel aluminum mini wind turbine." *Materials Today: Proceedings* 43 (2021): 1304-1312. https://doi.org/10.1016/j.matpr.2020.09.106
[13] Jamdade, Parikshit G., Santosh V. Patil, and Shrinivas G. Jamdade. "Assessment of power coefficient of an offline wind turbine generator system." *Electronic Journal of Energy & Environment* 1, no. 3 (2013). https://doi.org/10.7770/ejee-V1N3-art683
[14] Zawadzki, Karol, Wojciech Śmiechowicz, Małgorzata Stępień, Anna Baszczyńska, and Michał Tarkowski. "Influence of the solidity ratio on the small wind turbine aerodynamics." In *E3S Web of Conferences*, vol. 242, p. 03006. EDP Sciences, 2021. https://doi.org/10.1051/e3sconf/202124203006
[15] Hasan, Mahmoud E., Abdelgalil Eltayesh, Mohamed I. Awaad, and Hesham M. El-Batsh. "Experimental Examination for the Electric Power Generation of a Commercial Small-scale Wind Turbine with Modified Aerodynamic Design." *Alexandria Engineering Journal* 64 (2023): 25-39. https://doi.org/10.1016/j.aej.2022.08.040
[16] Ghorani, Mohammad Mahdi, Behrooz Karimi, Seyed Mohammad Mirghavami, and Zoheir Saboohi. "A numerical study on the feasibility of electricity production using an optimized wind delivery system (Invelox) integrated with a Horizontal axis wind turbine (HAWT)." *Energy* 268 (2023): 126643. https://doi.org/10.1016/j.energy.2023.126643
[17] Kamran, Muhammad. "Planning and Modeling of Wind Energy Systems." Fundamentals of Smart Grid Systems, 2023, 271–98. https://doi.org/10.1016/B978-0-323-99560-3.00003-X
[18] Mohanan, Janesh N., Kumaravel Sundaramoorthy, and Ashok Sankaran. "Performance improvement of a low-power wind turbine using conical sections." *Energies* 14, no. 17 (2021): 5233. https://doi.org/10.3390/en14175233
[19] Almohammadi, K. M., D. B. Ingham, L. Ma, and M. Pourkashan. "Computational fluid dynamics (CFD) mesh independency techniques for a straight blade vertical axis wind turbine." *Energy* 58 (2013): 483-493. https://doi.org/10.1016/j.energy.2013.06.012
[20] Stavrakakis, G. S., and A. Sayigh. "2.10-Electrical Parts of Wind Turbines." *Comprehensive Renewable Energy, Elsevier* (2012): 269-328. https://doi.org/10.1016/B978-0-08-087872-0.00211-0
[21] Lou, Bin, Zhilong Huang, Shangjun Ye, and Gaofeng Wang. "Experimental and numerical studies on aerodynamic control of NACA 4418 airfoil with a rotating cylinder." *Journal of Vibration Engineering & Technologies* 8 (2020): 141-148. https://doi.org/10.1007/s42417-019-00085-5
[22] Mahato, Arunabha, Ravi Kant Singh, Rahul Barnwal, and Subhas Chandra Rana. "Aerodynamic characteristics of NACA 0012 vs. NACA 4418 airfoil for wind turbine applications through CFD simulation." *Materials Today: Proceedings* (2023). https://doi.org/10.1016/j.matpr.2023.05.439
[23] Jafari, Seyed AH, and Buyung Kosasih. "Flow analysis of shrouded small wind turbine with a simple frustum diffuser with computational fluid dynamics simulations." *Journal of Wind Engineering and Industrial Aerodynamics* 125 (2014): 102-110. https://doi.org/10.1016/j.jweia.2013.12.001